Manipulation of the Pancharatnam phase in vectorial vortices

Avi Niv, Gabriel Biener, Vladimir Kleiner, Erez Hasman

Optical Engineering Laboratory, Faculty of Mechanical Engineering, Technion-Israel Institute of Technology, Haifa 32000, Israel
mehasman@tx.technion.ac.il

http://www.technion.ac.il/optics/

Abstract: Linearly polarized vectorial vortices are analyzed according to their Pancharatnam phase and experimentally demonstrated using a geometric phase element consisting of space-variant subwavelength gratings. It is shown that in the absence of a Pancharatnam phase, stable vectorial vortices that have no angular momentum arise. In contrast, if a Pancharatnam phase is present the vectorial vortices have orbital angular momentum and collapse upon propagation.

OCIS codes: (050.2770) Gratings; (260.5430) Polarization.

References and links

1. M. S. Soskin, M.V. Vasnetsov, "Singular optics," in *Progress in Optics, Vol.* **42**, E. Wolf ed. (Elsevier, Netherlands, Amsterdam, 2001), pp. 219-276.
2. D. Palacios, D. Rozas, and G. A. Swartzlander Jr., "Observed scattering into a dark optical vortex core," Phys. Rev. Lett. **88**, 103902 1-4 (2002).
3. J .F. Nye, "Polarization effect in the diffraction of electromagnetic waves: the role of disclinations," Proc. R. Soc. Lond. A **387**, 105-132 (1983).
4. J. F. Nye, "Lines of circular polarization in electromagnetic wave fields," Proc. R. Soc. London Ser. A **389**, 279-290 (1983).
5. J. V. Hajnal, "Singularities in the transverse fields of electromagnetic waves," Proc. R. Soc. Lond. A **414**, 433-446 and 447-468 (1987).
6. I. Freund, "Polarization singularity indices in Gaussian laser beams," Opt. Commun. **201**, 251-270 (2002).
7. M. R. Dennis, "Polarization singularities in paraxial vector fields: morphology and statistics," Opt. Commun. **213**, 201-221 (2002).
8. P. Pääkkönen, J. Tervo, P. Vahimaa, J. Turunen, and F. Gori, "General vectorial decomposition of electromagnetic fields with application to propagation-invariant and rotating fields," Opt. Express **10**, 949-959 (2002).
9. A. Niv, G. Biener, V. Kleiner, and E. Hasman, "Propagation-invariant vectorial Bessel beams obtained by use of quantized Pancharatnam-Berry phase optical elements," Opt. Lett. **29**, 238-240 (2004).
10. A. Niv, G. Biener, V. Kleiner, and E. Hasman, "Rotating vectorial vortices produced by space-variant subwavelength gratings," Opt. Lett. **30**, 2933-2935, (2005).
11. D. Mawet, P. Riaud, O. Absil, and J. Surdej, "Annular groove phase mask coronagraph," Astro. Phys. **633**, 1191-1200 (2005).
12. Y. Liu, D. Cline, and P. He, "Vacuum laser acceleration using a radially polarized CO_2 laser beam," Nucl. Instrum. Meth. Phys Res. A **424**, 296-303 (1999); W. D. Kimura, G. H. Kim, R. D. Romea, L. C. Steinhauer, I. V. Pogorelsky, K. P. Kusche, R. C. Fernow, X. Wang, and Y. Liu, "Laser acceleration of relativistic electons using the inverse Cherenkov effect," Phys. Rev. Lett. **74**, 546-549 (1995).
13. S. Quabis, R. Dorn, M. Eberler, O. Glöckl, and G. Leuchs, "Focusing light to a tighter spot," Opt. Commun. **179**, 1-7 (2000).
14. M. Stalder and M. Schadt, "Linearly polarized light with axial symmetry generated by liquid-crystal polarization converters," Opt. Lett. **21**, 1948-1950 (1996).
15. R. Oron, S. Blit, N. Davidson, A. A. Friesem, Z. Bomzon, and E. Hasman, "The formation of laser beams with pure azimuthal or radial polarization," Appl. Phys. Lett. **77**, 3322-3324 (2000).
16. K. C. Toussaint Jr., S. Park, J. E. Jureller, and N. F. Scherer, "Generation of optical vector beams with a diffractive optical element interferometer," Opt. Lett. **30**, 2846-2848 (2005).

#69636 - $15.00 USD Received 3 April 2006; revised 2 May 2006; accepted 2 May 2006

17. A. Niv, G. Biener, V. Kleiner, and E. Hasman, "Formation of linearly polarized light with axial symmetry by use of space-variant subwavelength gratings," Opt. Lett. **28,** 510-512 (2003).
18. Z. Bomzon, G. Biener, V. Kleiner, and E. Hasman, "Space-variant Pancharatnam-Berry phase optical elements with computer-generated subwavelength gratings," Opt. Lett. **27**, 1141-1143 (2002).
19. Q. Zhan and J. R. Leger, "Interferometric measurement of the geometric phase in space-variant polarization manipulations," Opt. Commun. **213**, 241-245 (2002).
20. E. Hasman, G. Biener, A. Niv, and V. Kleiner, "Space-variant polarization manipulation," in *Progress in Optics, vol.* **47**, E. Wolf ed. (Elsevier, Netherlands, Amsterdam, 2005), pp. 215-289.
21. L. Allen, M.J. Padgett, and M. Babiker, in *Progress in Optics, vol*. **39**, E. Wolf ed. (Elsevier, Netherlands, Amsterdam, 1999), pp. 291-372.
22. M. Born and E. Wolf, *Principles of Optics*, seventh ed. (Cambridge University Press, Cambridge, UK, 1999), Section 15.5.2.
23. R. C. Enger and S.K. Case, "Optical elements with ultrahigh spatial-frequency surface corrugations," Appl. Opt. **22** 3220-3228 (1983).
24. L. H. Cescato, E. Gluch, and N. Streibl, "Holographic quarterwave plates," Appl. Opt. **29** 3286-3290 (1990).
25. A. Niv, G. Biener, V. Kleiner, and E. Hasman, "Spiral phase elements obtained by use of discrete space-variant subwavelength gratings," Opt. Commun. **251**, 306–314 (2005).
26. S. Pancharatnam, "Generalized theory of interference and its applications. Part I. Coherent pencils," Proc. Ind. Acad. Sci. A **44** (1956) 247 [reprinted in S. Pancharatnam, *Collected Works* (Oxford University Press, 1975)].
27. P. K. Aravind, "A simple proof of Pancharatnam's theorem," Opt. Commun. **94**, 191-196 (1992); C. Brosseau, *Fundamentals of Polarized Light* (Wiley, New York, 1998).
28. E. Collett, *Polarized Light* (Marcel Dekker, New York, 1993).

1. Introduction

Singularities in scalar wave fields appear at points or along lines where the phase or the amplitude of the wave is either undefined or changes abruptly. An important type of singularity is the scalar vortex. A scalar vortex occurs where the phase of the scalar wave has a spiral structure around a singular point in the field [1]. Until now, research had focused mainly on this type of singularity [2]. However, if we allow the polarization to be space varying, vectorial vortices can be generated [3-7]. A vectorial vortex occurs around a point where a scalar vortex is centered in at least one of the scalar components of the vectorial wave field. Vectorial vortices can be found in the fields proposed by Pääkkönen et al. [8], at the center of vectorial Bessel beams [9] as well as at the center of a recently proposed phenomenon – rotating vectorial vortices [10]. It is expected that vectorial vortices will find application in advanced optical schemes such as phase mask coronagraphy [11], particle acceleration [12], and the tight focusing of light beams [13]. Vectorial vortices can be achieved by several means: liquid crystal devices [14], the intracavity summation of laser modes [15], interferometric techniques [16], and space-variant subwavelength gratings [9,10,17].

This paper experimentally studies and analyzes linearly polarized vectorial vortices by use of geometric phase elements. It is argued that the Pancharatnam phase is a prominent structural feature of these fields, where the Pancharatnam phase is the argument of the inner product of distinctly polarized waves [18,19]. We show that linearly polarized vectorial vortices that have no Pancharatnam phase are stable upon propagation and have no angular momentum. However, if a Pancharatnam phase is present, then the linearly polarized vectorial vortices have orbital angular momentum and collapse upon propagation. The vectorial vortices are achieved by use of discretely oriented space-variant subwavelength gratings. These devices employ a geometric Pancharatnam phase that results from space-variant polarization state manipulation [20]. The structure and properties of linearly polarized vectorial vortices are reviewed in chapter 2. The design and fabrication of the space-variant subwavelength gratings used to generate these vectorial vortices are described in chapter 3. The gratings were realized on GaAs wafers and illuminated by CO_2 laser radiation of $10.6\mu m$ wavelength. Chapter 4 describes the experimental demonstration verifying the theoretical analysis of the vectorial vortices generated by these space-variant subwavelength gratings.

#69636 - $15.00 USD Received 3 April 2006; revised 2 May 2006; accepted 2 May 2006

This verification was achieved by measuring the full polarization state at the immediate outlet of the devices, and at their Fraunhofer diffraction. Our concluding remarks are presented in Chapter 5.

2. Theory

2.1 The structure of vectorial vortices and their Pancharatnam phase

The most general polarization state of a linearly polarized vectorial vortex can be written as

$$\left|E\right\rangle = \frac{1}{\sqrt{2}}\exp\left(im\varphi + i\varphi_0/2\right)\left|R\right\rangle + \frac{1}{\sqrt{2}}\exp\left(in\varphi - i\varphi_0/2\right)\left|L\right\rangle, \tag{1}$$

where m and n are integers, $\left|R\right\rangle$ and $\left|L\right\rangle$ are the right- and left-handed polarization unit vectors, respectively, and φ is the angle in the polar coordinate system (r,φ). Equation (1) is consistent with the definition of a vectorial vortex as defined above [10]. The linearity of the field is secured by having equal magnitudes of the circularly polarized components, while φ_0 represents arbitrary retardation. As linearly polarized vortices are the sole topic of this paper, the term "vectorial vortex" will henceforth serve as the abbreviation for "linearly polarized vectorial vortices". Figure 1 illustrates the polarization state of vectorial vortices with different values of m and n, with $\varphi_0 = 0$; the polarization ellipses have degenerated and thus appear as bars. Usually, vectorial singularities are studied by looking at the temporal evolution of the field [3,4], however for brevity's sake, we have consigned this discussion to Appendix A.

An effective way to understand the structure of a field is to study its Pancharatnam phase [17]. The Pancharatnam phase between two distinctly polarized waves $\left|A\right\rangle$ and $\left|B\right\rangle$ is defined according to $\varphi_P = \arg\langle A|B\rangle$. Note that a π phase of indeterminate sign appears in φ_P across point where $\langle A|B\rangle = 0$. However, as these steps are of no special physical significance, they will be omitted from the following discussion altogether. Taking $\left|E(\varphi=0)\right\rangle$ as a reference, the Pancharatnam phase of the vectorial vortex is given by

$$\varphi_P = \arg(\langle E(\varphi=0)|E(\varphi)\rangle) = \frac{m+n}{2}\varphi. \tag{2}$$

Therefore, linearly polarized waves at different azimuthal locations across the field are not only rotated with respect to each other according to $(m\text{-}n)\varphi/2$, [as calculated from Eq. (1)], but are also advanced or retarded according to Eq. (2).

This result is easily observed by presenting Eq. (1) in the Cartesian basis explicitly as,

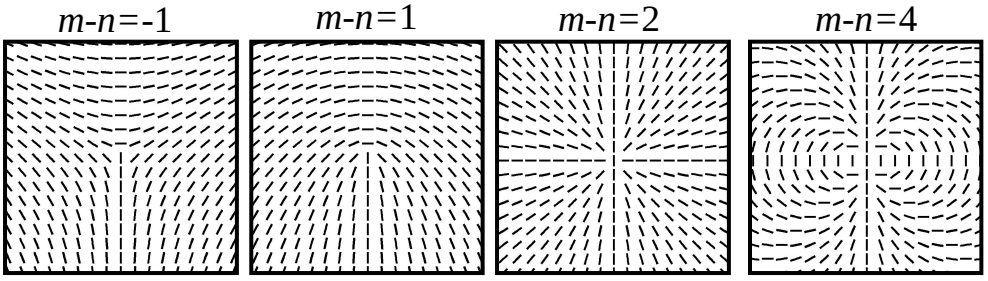

Fig. 1. Azimuthal angle distribution of the polarization state for vectorial vortices with m-n equal -1, 1, 2 and 4 (from left to right).

#69636 - $15.00 USD Received 3 April 2006; revised 2 May 2006; accepted 2 May 2006

$$\left|E\right\rangle = \begin{pmatrix} \cos\left(\frac{m-n}{2}\varphi + \frac{\varphi_0}{2}\right) \\ \sin\left(\frac{m-n}{2}\varphi + \frac{\varphi_0}{2}\right) \end{pmatrix} \exp\left(i\frac{m+n}{2}\varphi\right). \tag{3}$$

The rotation is indicated by the Jones vector, and the Pancharatnam phase is equal to the phase inside the exponent. In appendix A, we show that the Pancharatnam phase is also in agreement with the temporal behavior of the field.

Topological charges are an important aspect of scalar vortices as they are directly related to the orbital angular momentum of canonical vortices [21]. In this study, we attempt to associate a topological charge with the vectorial vortex. We show that there is a correlation between the topological charge of the vectorial vortex and its angular momentum. In scalar fields, topological charges are defined according to the number of 2π radians that the phase of the scalar wave accumulates along a closed path surrounding the singularity. The topological charge of the vectorial vortex is defined in the same manner, but uses the Pancharatnam phase instead of the scalar phase. Thus,

$$l_P = \frac{1}{2\pi}\oint_C d\varphi_P \,, \tag{4}$$

where the integration path, *C*, encircles the phase singularity. We denote the topological charge of the vectorial vortex as a topological Pancharatnam charge. Applying Eq. (2) to Eq. (4), the topological Pancharatnam charge of the vectorial vortex is $l_P=(m+n)/2$. To establish the connection between l_P and the angular momentum of the vectorial vortex, let us first calculate the total angular momentum of the vectorial vortex as the sum of the orbital angular momentum of its scalar components. The spin angular momentum is canceled out as indicated by Eq. (1). This calculation results in a normalized angular momentum of,

$$\frac{J_z}{P} = \frac{m+n}{2\omega}, \tag{5}$$

where *P* is the total intensity of the field and ω is the optical frequency. Comparing this result to the expression for the topological Pancharatnam charge of a vectorial vortex, we find,

$$\frac{J_z}{P} = \frac{l_P}{\omega}. \tag{6}$$

Therefore, the topological Pancharatnam charge, with respect to the orbital angular momentum of vectorial vortices is analogous to the topological charge of scalar vortices.

From Eq. (1), the Fraunhofer diffraction of a vectorial vortex is given by,

$$\left|E_{fh}(r,\varphi,z)\right\rangle = \frac{k\exp(ikz)}{\sqrt{2}z}\left\{\left[i^{m-1}\exp\left[i\left(m\varphi+\varphi_0/2\right)\right]\int_0^R J_m\left(krr'/z\right)r'dr'\right]\left|R\right\rangle + \left[i^{n-1}\exp\left[i\left(n\varphi-\varphi_0/2\right)\right]\int_0^R J_n\left(krr'/z\right)r'dr'\right]\left|L\right\rangle\right\}. \tag{7}$$

Here, *z* is the propagation distance, *k* is the wavenumber, and *R* corresponds to the radius of the finite aperture of the field. Equation (7) shows that the components of the vectorial vortex undergo different modulations as the distance *z* is increased. As a result, a vectorial vortex does not maintain its structure upon propagation. However, in the unique case where no

#69636 - $15.00 USD Received 3 April 2006; revised 2 May 2006; accepted 2 May 2006

Pancharatnam phase is present, i.e., n = - m [see Eq. (2)], Eq. (7) reduces to,

$$\left|E_{fh}(r,\varphi,z)\right\rangle = \frac{k\exp(ikz)i^{m-1}}{z}\begin{pmatrix}\cos(m\varphi+\varphi_0)\\ \sin(m\varphi+\varphi_0)\end{pmatrix}\int_0^R J_m(krr'/z)r'dr'. \qquad (8)$$

In this special case, the vectorial vortex maintains its polarization structure upon propagation. From Eq. (7) and (8) we conclude that fields with Pancharatnam phases other than zero do not maintain their polarization structure upon propagation, while the polarization state of fields with no Pancharatnam phase is stable.

2.2 Geometric phase elements

Vectorial vortices are easily generated using discretely oriented space-variant subwavelength gratings. It is well known that when the period of a dielectric grating is smaller than the incident wavelength, only the zero diffraction order is propagating and all the other orders are evanescent. In this case, the grating behaves as a uniaxial crystal with the optical axes parallel and perpendicular to the subwavelength grooves [22-24]. By fabricating a subwavelength grating in which the groove orientation varies along the face of the element, a space-variant wave plate is realized. We have previously shown [25] that the field emerging from such a device is given by,

$$\left|E_{out}\right\rangle = \frac{1}{2}(t_x + t_y e^{i\phi})\left|E_{in}\right\rangle + \frac{1}{2}(t_x - t_y e^{i\phi})\left[e^{i2\theta}\left|R\right\rangle\left\langle L\right|E_{in}\right\rangle + e^{-i2\theta}\left|L\right\rangle\left\langle R\right|E_{in}\right\rangle], \qquad (9)$$

where $\left|E_{in}\right\rangle$ represents the beam impinging on the device and $\theta=\theta(x,y)$ is the local orientation of the subwavelength grooves. t_x, t_y are the amplitude transmission coefficients for light polarized perpendicular and parallel to the subwavelength grooves, respectively, and ϕ is the retardation phase. Equation (9) indicates that the field emerging from a space-variant subwavelength grating comprises three components. The first maintains the original polarization state and phase of the incoming beam. The second is right-handed circularly polarized and has a phase modification of $2\theta(x,y)$. The third has an orthogonal polarization direction and opposite phase modification with respect to the second component. Note that the magnitude of the different components is determined by the local birefringent parameters t_x, t_y and ϕ, as well as by the incoming polarization state for the second and third components. The transmission of dielectric gratings is relatively high and the retardation ϕ is primarily a function of the subwavelength grooves etching depth. Therefore, we consider devices with subwavelength grooves for which $t_x \approx t_y \approx 1$ and $\phi = \pi$ or $\pi/2$, i.e. perfect space-variant half and quarter wave plates.

Let us consider a local orientation of the subwavelength grooves as,

$$\theta = \frac{m\varphi}{2} + \theta_0 \ (m \text{ is an integer}). \qquad (10)$$

The beam emerging from a space-variant subwavelength grating with this groove orientation, where $\theta_0=\phi/2$, $t_x=t_y=1$, and $\phi=\pi$, for linearly polarized illumination is,

$$\left|E_{out}\right\rangle = \frac{1}{\sqrt{2}}\left[e^{im\varphi}\left|R\right\rangle + e^{-im\varphi}\left|L\right\rangle\right]. \qquad (11)$$

This field resembles Eq. (1) for n = -m. Thus, a vectorial vortex with field vectors which has no Pancharatnam phase is produced. From the discussion in chapter 2.1, this vectorial vortex exhibits no orbital angular momentum and has beam-like propagation.

Another possibility for generating vectorial vortices using space-variant subwavelength gratings is obtained once a circularly polarized plane wave impinges a device, acting as a perfect quarter wave plate, i.e., $t_x=t_y=1$ and $\phi=\pi/2$, with subwavelength groove orientation

#69636 - $15.00 USD Received 3 April 2006; revised 2 May 2006; accepted 2 May 2006

given by Eq. (10). In this case, if $\theta_0=\pi/4$ and the illuminating beam is left- handed circularly polarized, then according to Eq. (9) the emerging field is

$$\left|E_{out}\right\rangle = \frac{1}{\sqrt{2}}\left[e^{im\varphi}\left|R\right\rangle + \left|L\right\rangle\right]. \tag{12}$$

This field resembles Eq. (1) for $n = 0$. This is a vectorial vortex with Pancharatnam phase of helical structure, thus $\varphi_p=m\varphi/2$ as can be calculated from Eq. (2). From Eq. (5), this vectorial vortex has an orbital angular momentum of $\hbar m/2$ per photon. However, from Eq. (7), we find that it does not maintain its polarization structure upon propagation. Note, in case of $m=\pm 1$ the central singularity is a generic feature of vectorial fields known as C-point [4]. In both cases, θ_0 is of no special importance apart from the case of the space-variant quarter wave plate with $m=2$.

In the case of vectorial vortices that are generated by space-variant subwavelength gratings, the Pancharatnam phase results from the space-variant polarization state manipulations and is therefore geometric in nature. This is best understood by viewing the polarization state manipulations involved in the formation of the vectorial vortices on a Poincaré sphere. A Poincaré sphere is a unit sphere for which the normalized Stokes parameters $\hat{s}_1$, $\hat{s}_2$, $\hat{s}_3$ serve as rectangular coordinates [26]. In this representation, a specific polarization state is mapped to a point on the sphere, while polarization state transformations are represented by geodesic lines connecting the initial and final polarization states. Let us consider the geodesic triangle ABC of Fig. 2(a) using similar calculations to those performed by Aravind [24]. It can be shown that if a wave in a state A is in phase with a distinctly polarized wave B, and if A is also in phase with another wave at polarization state C, then the waves at states B and C are not necessarily in phase. In fact, the phase between them equals half the area of the geodesic triangle ABC and is therefore geometric in nature [27].
Fig. 2(b) shows a mapping of the polarization state transformation of the vectorial vortex of Eq. (11) onto a Poincaré sphere. The incoming polarization state (point A on the sphere) as well as the emerging polarization states at different locations are linear with different orientations (points B and C on the sphere). In this case, the Pancharatnam phase between the states A and B, and A and C is zero. As the geodesic triangle ABC encompasses a null area, no geometric phase is obtained between the states B and C.

The case of the vectorial vortex of Eq. (12) is depicted in Fig. 2(c). Here, the incoming wave (point A on the sphere) is left-handed circularly polarized, while the emerging field at different locations is linearly polarized with different orientations (points B and C on the sphere). It is easy to show (using Eq. (1) or Eq. (3) with $n=0$ and $\varphi_0=0$) that in this case as well, A is in phase with B and with C. According to the geometric considerations given in

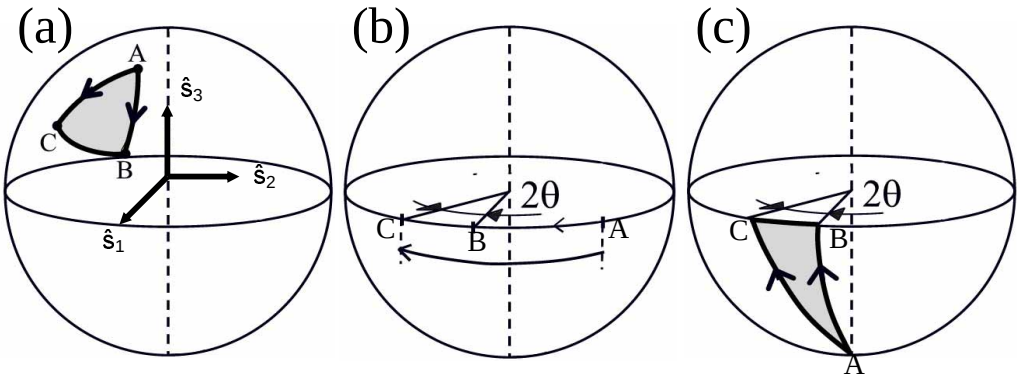

Fig. 2. Mapping of the polarization state manipulation onto a Poincaré sphere. (a) In an arbitrary case, (b) for the formation of a vectorial vortex without a Pancharatnam phase, (c) for the formation of a vectorial vortex with a Pancharatnam phase.

#69636 - $15.00 USD Received 3 April 2006; revised 2 May 2006; accepted 2 May 2006

Ref. 27, we find the area of the geodesic triangle ABC (shaded in the figure) to be $m\varphi$ stradians. Therefore, a geometric phase that equals half the area enclosed on the Poincaré sphere by the geodesic lines is added to the wave at C with respect to B. Comparing these results with Eq. (2), we conclude that vectorial vortices that are generated by space-variant subwavelength gratings have an entirely geometric Pancharatnam phase.

3. Design and realization of subwavelength gratings for the generation of vectorial vortices

In order to overcome the customary limitations of continuous space-variant subwavelength gratings [17], in our approach [25], the desired groove orientation of Eq. (10) is approximated by,

$$\theta(x,y)\big|_{\mathrm{mod}\,\pi} = F_N\left[(m\varphi/2+\theta_0)\right] \ (m \text{ is an integer}). \tag{13}$$

The function $F_N()$ denotes a piecewise process that divides a desired groove orientation into N equal zones. The discontinuities in the subwavelength pattern unavoidably lead to diffraction. The efficiency of the first diffraction order is given by [25],

$$\eta_1 = \left[\frac{N}{\pi}\sin\left(\frac{\pi}{N}\right)\right]^2. \tag{14}$$

This equation indicates that for 2, 4, 8, and 16 discrete steps, the first order diffraction efficiency is 40.5%, 81.1%, 95.0%, and 98.7%, respectively. As the first order represents an

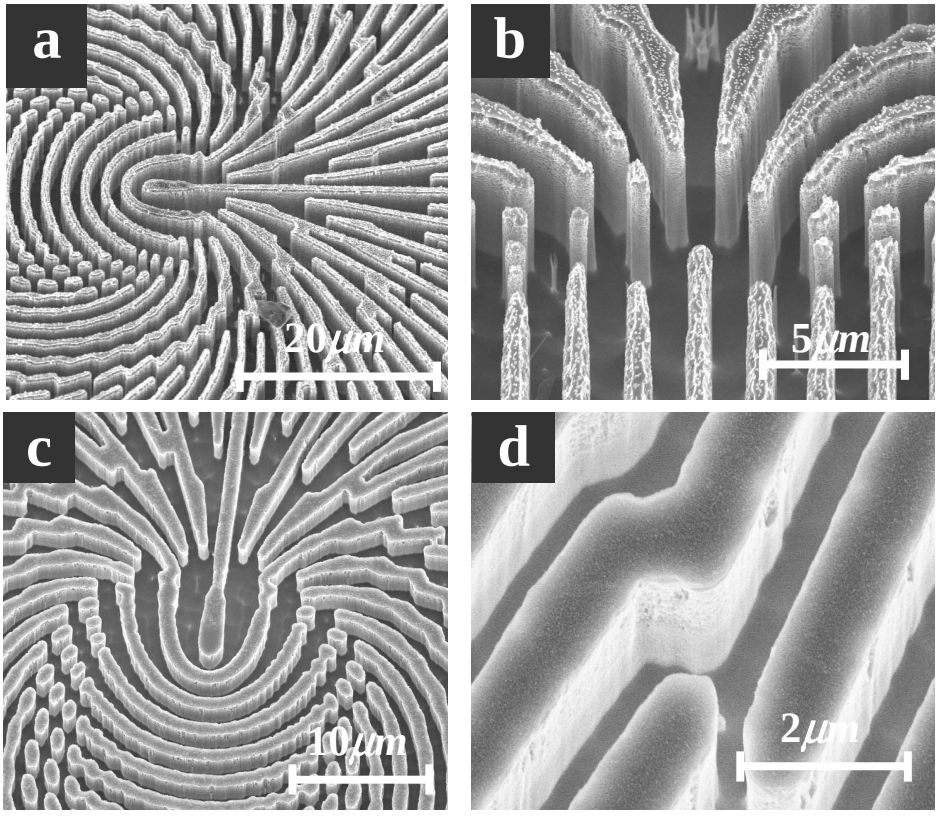

Fig. 3. Scanning electron microscope images (a) of a π-retardation device with a nominal etching depth of 5μm and m=3 (b) of a π-retardation device for m=4 (c) of a $\pi/2$- retardation device with 2.5μm nominal etching depth and m=3, (d) with higher magnification of the $\pi/2$-retardation device. The local period of the depicted gratings is 2μm.

#69636 - $15.00 USD Received 3 April 2006; revised 2 May 2006; accepted 2 May 2006

exact replica of our desired continuous field, an almost perfect device can be achieved by merely using $N = 16$ [25]. High-resolution laser lithography chrome masks as generated using Eq. (13) for $\theta_0=\pi/4$ and $m = 1, 2, 3, 4$ were fabricated. The masks were 10mm in diameter and had $N = 16$ zones. A subwavelength period of $\Lambda=2\mu m$ was chosen along with a fill factor of 0.5 for use with
$10.6\mu m$ wavelength radiation. The masks were transferred by contact lithography to $500\mu m$ thick GaAs wafers and space-variant subwavelength gratings were achieved using the fabrication process described in Ref. 25. The nominal etching depths were $2.5\mu m$ and $5\mu m$, in order to achieve the desired $\pi/2$ and π–retardation, respectively. As a final step, the backsides of the elements were applied with an anti-reflection coating. Figure 3 shows scanning electron

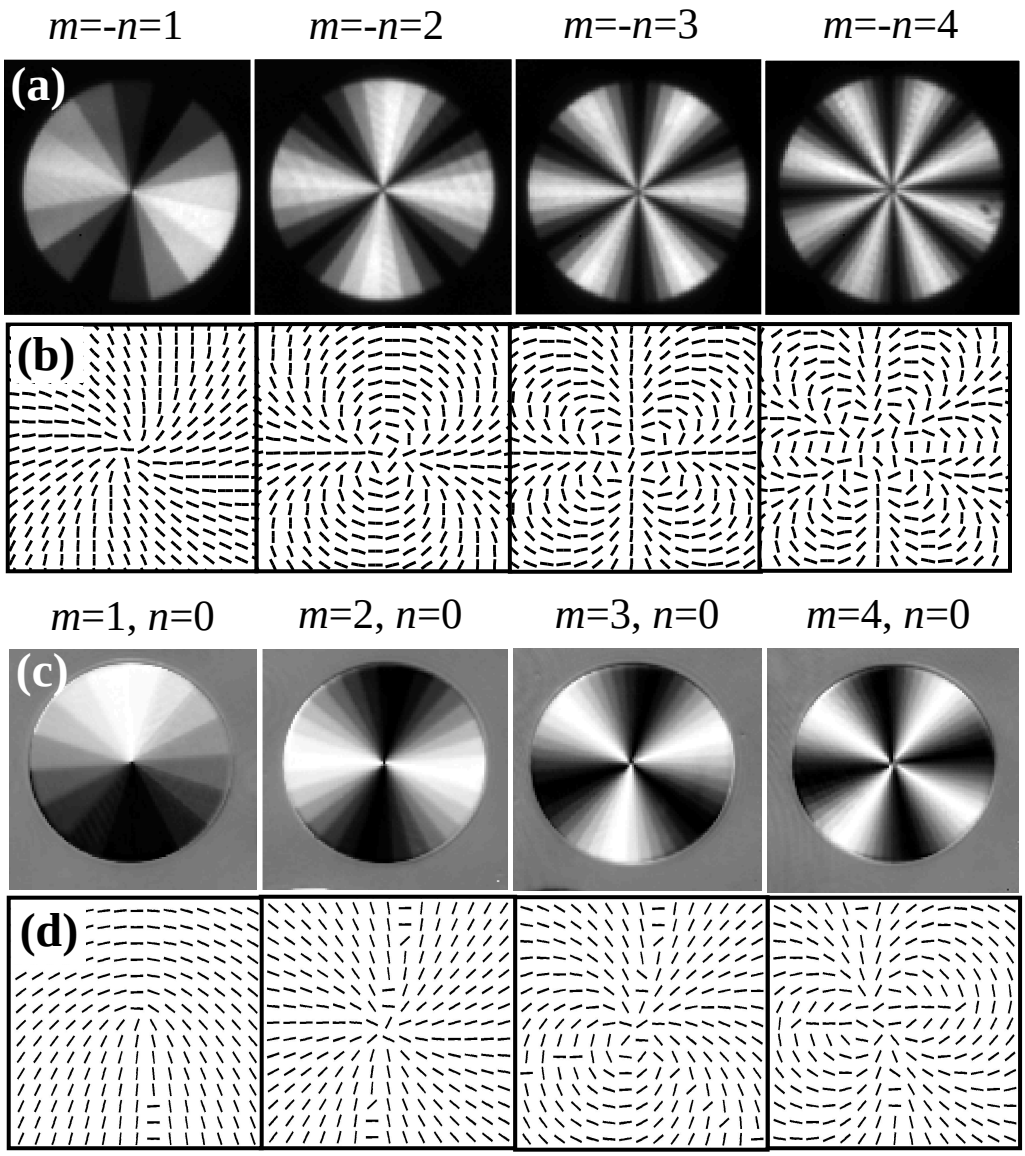

Fig. 4. Measured intensity distributions for vectorial vortices imaged through a linear polarizer immediately behind the elements, (a) without Pancharatnam phase and (c) with Pancharatnam phase. (b), (d) Measured azimuthal angle distributions for the corresponding cases.

#69636 - $15.00 USD Received 3 April 2006; revised 2 May 2006; accepted 2 May 2006

microscope images of the devices. Discrete changes in the groove orientation as well as the high aspect ratio and rectangular shape of the grooves are clearly observed. For a device with nominal retardation of π radians, we have previously measured the amplitude transmission to be t_x = 0.74 and t_y = 0.86, with actual retardation of $\phi = 0.97\pi$ [25], thus high efficiency devices are formed using the prescribed process. Fig. 4: Measured intensity distributions for vectorial vortices imaged through a linear polarizer immediately behind the elements, (a) without Pancharatnam phase and (c) with Pancharatnam phase. (b), (d) Measured azimuthal angle distributions for the corresponding cases.

4. Experimental results

Vectorial vortices that do not have a Pancharatnam phase were obtained by illuminating the π-retardation devices with 10.6μm linearly polarized light from a CO_2 laser. Figure 4(a) shows the intensity distributions at the immediate outlet of the devices when imaged through a linear polarizer. The fringes indicate the rotation of the polarization ellipses according to Eq. (3) for $n = -m$. We have measured the polarization state distribution of the vectorial vortices using the four-measurement technique [28]. Figure 4(b) shows the azimuthal angle distribution. The rotation around the field axis is clearly observed. We have found the typical deviation of the azimuthal angle with respect to its desired value to be less than 2% (0.026 radians). The typical ellipticity of the emerging field was less than 0.07 radian. This result is comparable with the expected performance of a device with N=16, indicating the excellent ability of a space-variant subwavelength grating to control the polarization state of a beam. Vectorial

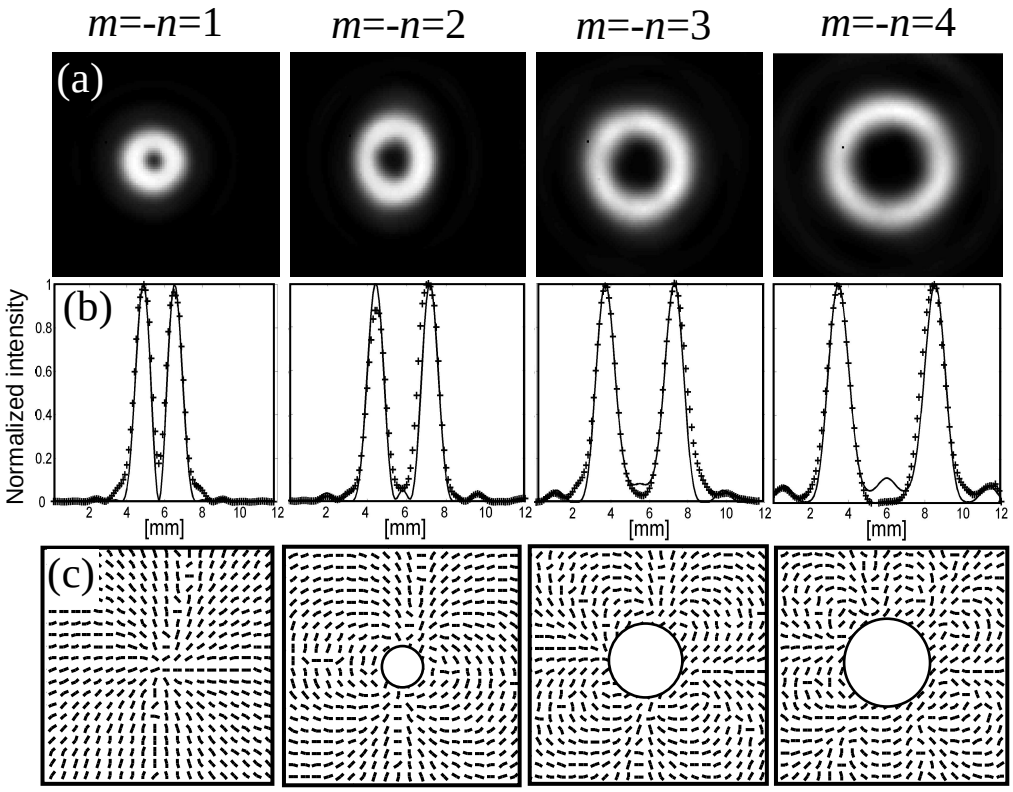

Fig. 5. (a) Measured intensity distributions at the Fraunhofer region for vectorial vortices without Pancharatnam phases. (b) Typical cross sections of the intensity distribution in (a) (crosses represent experimental measurements while solid lines represent calculations). (c) Measured azimuthal angle distributions of the vectorial vortices' polarization states.

#69636 - $15.00 USD Received 3 April 2006; revised 2 May 2006; accepted 2 May 2006

vortices having a Pancharatnam phase were obtained by illuminating the π/2-retardation devices with 10.6μm left-handed circularly polarized light from a CO_2 laser. Figure 4(c) shows the intensity distributions at the immediate outlet of the devices imaged through a linear polarizer. In this case, the fringes indicate rotation of the polarization ellipses that is in agreement with Eq. (3) for n=0. Figure 4(d) shows the measured azimuthal angle in this case. Typical values for the deviation of the azimuthal angle and ellipticity, compared to their desired value, are similar to the former case, thus indicating the formation of high quality vectorial vortices.

4.1 Fraunhofer diffraction of vectorial vortices without Pancharatnam phase

The Fraunhofer diffraction of the vectorial vortices that do not have a Pancharatnam phase (i.e., n=-m) were obtained at the focus of a lens with 1m focal length. Figure 5(a) shows their measured intensity distributions. The annular intensity pattern that is predicted by Eq. (8) is clearly observed. Another way to understand this is to average the fields located on a circle surrounding the singularity and limiting the circle radius to 0, thus

$$\tilde{E} = \lim_{r\to 0} \int_0^{2\pi} \left| E(r,\varphi) \right\rangle d\varphi \,, \tag{15}$$

where the field, $E(r,\varphi)$, is calculated from Eq. (8). This average, in the presented case, results in $\tilde{E}=(0,0)^T$, where T denotes transposition. Thus, the dark core is a result of destructive interference of the field at the center. This outcome is also predicted by Eq. (1), when

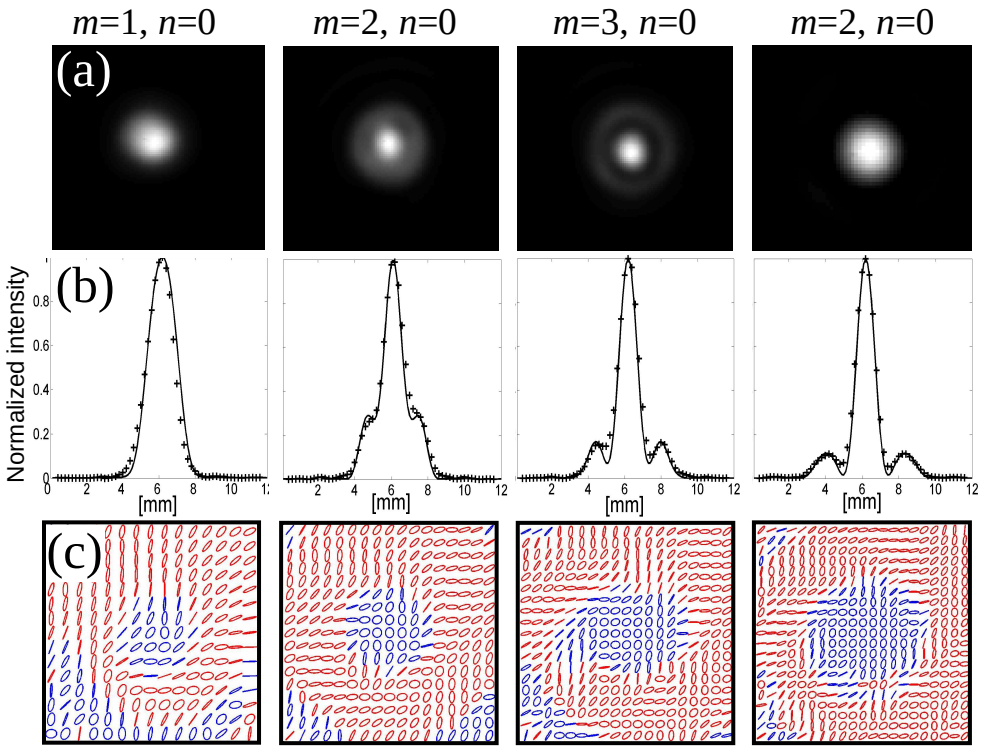

Fig. 6. (a) Measured intensity distributions at the Fraunhofer region for vectorial vortices with Pancharatnam phase, obtained with a π/2-retardation device. (b) Typical cross sections of the intensity distribution in (a) (crosses represent experimental measurements, while solid lines represent calculated values), (c) measured polarization ellipse distribution of the vectorial vortices. The colors indicate the different rotation directions (handedness) of the field.

#69636 - $15.00 USD
Received 3 April 2006; revised 2 May 2006; accepted 2 May 2006

considering conjugate scalar vortices embedded in both orthogonally polarized components of the vectorial vortex. Typical cross sections of the intensity distributions are given in Fig. 5(b). Good agreement between the experimental results and the theoretical analysis is obtained. Moreover, Fig. 5(c) shows the measured space-variant azimuthal angle of the beam's polarization state at the Fraunhofer region. The close resemblance of the polarization states between the near- and the far-fields validates our conclusion that vectorial vortices that do not have a Pancharatnam phase maintain their structure upon propagation.

4.2 Fraunhofer diffraction of vectorial vortices with Pancharatnam phase

Fraunhofer diffraction of vectorial vortices that have a Pancharatnam phase were obtained at the focus of a lens with 1*m* focal length, and are shown in Fig. 6(a). In this case, n=0 and a bright spot at the center of the field is observed. The bright central spots are also shown in the typical cross sections of Fig. 6(b). These bright central spots (as well as the annular intensity rings) are anticipated from Eq. (7) for $n = 0$. This results from the constructive interference at the center of the field. The central spots' polarization state can be found by applying Eq. (7) to Eq. (15), yielding $\tilde{E} \propto |L\rangle$. The measured polarization ellipses of the far-field vectorial vortices are shown in Fig. 6(c). Different colors indicate different handedness of the field. At the boundary between handedness, there is a line of linear polarization known as an L-line [6]. At the center of the field, there are points of circular polarization known as C-points [7]. One can see that the polarization state is radically different from the polarization state of the beam emerging from the element. In other words, the polarization state of the propagated beam is not a linearly polarized axially symmetric vectorial vortex. Therefore the vectorial vortex collapses upon propagation, as discussed in chapter 2. Experimental evaluation of the central spot showed its polarization state to be left-handed circularly polarized, as anticipated from Eqs. (7) and (15). Good agreement between theory and experimental results, as can be seen from Fig. 6, is demonstrated.

4.3 Fraunhofer diffraction of general vectorial vortex

We have also demonstrated a vectorial vortex with $m,n \neq 0$as well as $m \neq -n$, (see Eq. (1) that has a Pancharatnam phase, by combining a spiral phase element with a scalar topological charge, l, immediately behind the π-retardation device. In this case, a phase of $l\varphi$ is added to both components of the beam producing

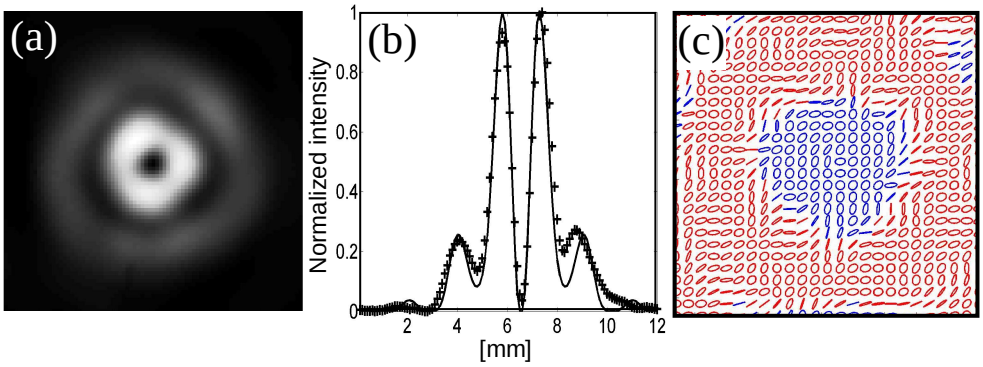

Fig. 7. (a) Measured intensity distribution at the Fraunhofer region for a vectorial vortex with Pancharatnam phase, obtained with a π-retardation device of m=3 and a spiral phase element with a topological charge of l=2. (b) Typical cross-section taken from the intensity distribution in (a) (crosses represent experimental measurements, while solid line represents calculated values). (c) Measured polarization ellipse distribution of the vectorial vortex. The colors indicate the different rotation directions (handedness) of the field.

#69636 - $15.00 USD Received 3 April 2006; revised 2 May 2006; accepted 2 May 2006

$$|E\rangle = \frac{1}{\sqrt{2}}\exp[i(m+l)\varphi]|R\rangle + \frac{1}{\sqrt{2}}\exp[-i(m-l)\varphi]|L\rangle \cdot \quad (16)$$

Equation (16) shows that any desired linearly polarized vectorial vortex can be obtained by combining a spiral helical phase element with a discretely oriented space-variant subwavelength grating-based device. The vectorial vortex was achieved experimentally by combining a spiral phase element with l=2 and a π-retardation device of m=3. The spiral phase element was formed by a 32-level reactive-ion etching on a ZnSe substrate. Figures 7(a) and 7(b) show the Fraunhofer diffraction intensity distribution of the measured vectorial vortex, as well as its measured and predicted cross sections. As can be seen from these figures, the dark central spot is obvious, as anticipated by Eqs. (7) and (15). The measured polarization ellipses of this field are shown in Fig. 7(c). As in Fig. 6, the L-line at the boundary between different handedness is clearly shown. We have measured the polarization states of both intensity rings to be left- and right-handed circularly polarized, for the inner and outer rings, respectively. This result agrees with Eq. (7). As can be seen, the measured polarization state is no longer a linearly polarized axially symmetric vectorial vortex. Hence, a vectorial vortex with a Pancharatnam phase collapses upon propagation, as discussed in chapter 2.

5. Conclusions

Two types of linearly polarized vectorial vortices were discussed and demonstrated. The first type which had no Pancharatnam phase showed no angular momentum and maintained its structure upon propagation. The second type had a Pancharatnam phase of helical structure, had orbital angular momentum, and collapsed upon propagation. From these results, we

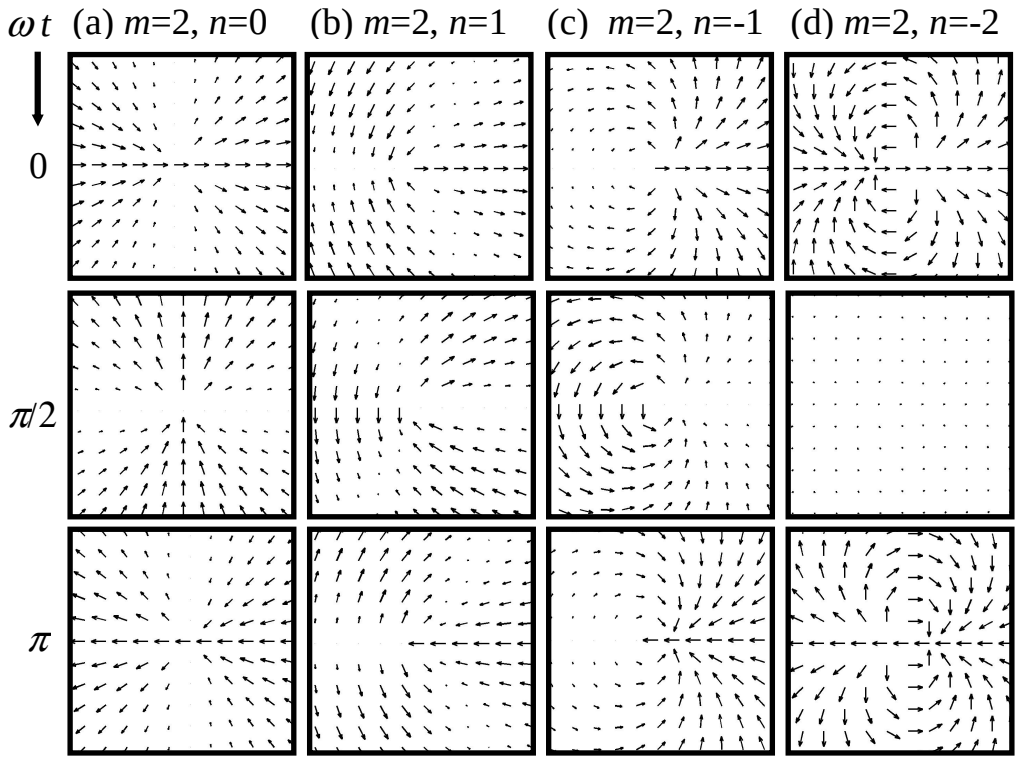

Fig 1A. Calculated real part of the instantaneous vector fields for several linearly polarized vectorial vortices.

#69636 - $15.00 USD Received 3 April 2006; revised 2 May 2006; accepted 2 May 2006

conclude that the Pancharatnam phase of vectorial vortices is an essential property that influences the propagation of such fields. The vectorial vortices were demonstrated using discretely oriented space-variant subwavelength gratings. These devices have proven to be able to produce high quality vectorial vortices that are also highly efficient.

Appendix A – The temporal evolution of the vectorial vortex

From a physical point of view, it is not the complex field of Eq. (1) that is important but the real time dependent field given by,

$$\mathrm{Re}\left[\left|E\right\rangle \exp(-i\omega t)\right] = \begin{pmatrix} \cos\left(\frac{m-n}{2}\varphi + \frac{\varphi_0}{2}\right) \\ \sin\left(\frac{m-n}{2}\varphi + \frac{\varphi_0}{2}\right) \end{pmatrix} \cos\left(\frac{m+n}{2}\varphi - \omega t\right). \tag{1A}$$

The temporal dependence indicates the existence of $m+n$ lines of zero magnitude rotating at $2\omega/(m+n)$ radian per second. These zero lines are known as disclinations [4]. The temporal evolution of these fields is illustrated in Fig. 1A for different values of m and n. Note in Figs. 1A (a) - (c) that the orientation of the field vector and the lines of zero magnitude obey Eq. (1A). However, special attention should be given to particular cases. First, if $m = -n$, no rotating zero lines appear, but rather the field vectors vanish simultaneously, as can be seen in Fig. 1A(d). The second case is $m = n$, which corresponds to a uniformly oriented linearly polarized field. This case was vastly treated within the framework of scalar singular optics, thus it is omitted from the current discussion. The temporal evolution is in agreement with the concept of the Pancharatnam phase of the field. Equation (2) shows that the Pancharatnam phase advances the wave in a helical manner around the field axis, causing the location of instantaneous zeros to rotate in time, as shown in Figs. 1A(a-c). In the particular case where $m = -n$, the Pancharatnam phase is zero, and thus the beating of the waves are synchronized in time and the field vanishes simultaneously, as can be seen in Fig. 1A(d).

#69636 - $15.00 USD Received 3 April 2006; revised 2 May 2006; accepted 2 May 2006